



RESEARCH ARTICLE

10.1029/2022JD037749

Key Points:

- Continuous observations of atmospheric gaseous elemental mercury (GEM) show significant decreasing trends over the past 5–7 years
- Slight increase of $\delta^{202}\text{Hg}$ and decrease of $\Delta^{199}\text{Hg}$ and $\Delta^{200}\text{Hg}$ with decreasing GEM concentration are observed
- Changes in GEM concentrations and isotope compositions are mainly driven by reduced anthropogenic emissions

Supporting Information:

Supporting Information may be found in the online version of this article.

Correspondence to:

X. Fu and X. Feng,
fuxuewu@mail.gyig.ac.cn;
fengxinbin@vip.gyig.ac.cn

Citation:

Wu, X., Fu, X., Zhang, H., Tang, K., Wang, X., Zhang, H., et al. (2023). Changes in atmospheric gaseous elemental mercury concentrations and isotopic compositions at Mt. Changbai during 2015–2021 and Mt. Ailao during 2017–2021 in China. *Journal of Geophysical Research: Atmospheres*, 128, e2022JD037749. <https://doi.org/10.1029/2022JD037749>

Received 28 AUG 2022

Accepted 12 MAY 2023

Author Contributions:

Conceptualization: Xuewu Fu, Xinbin Feng

Formal analysis: Xian Wu, Xuewu Fu, Kaihui Tang, Xun Wang, Hui Zhang, Qianwen Deng

Investigation: Xian Wu, Xuewu Fu, Hui Zhang, Kaihui Tang





Methodology: Xian Wu, Xuewu Fu, Hui Zhang

Resources: Kaiyun Liu, Qingru Wu, Shuxiao Wang

© 2023. The Authors.

This is an open access article under the terms of the [Creative Commons Attribution License](https://creativecommons.org/licenses/by/4.0/), which permits use, distribution and reproduction in any medium, provided the original work is properly cited.

Changes in Atmospheric Gaseous Elemental Mercury Concentrations and Isotopic Compositions at Mt. Changbai During 2015–2021 and Mt. Ailao During 2017–2021 in China

Xian Wu^{1,2}, Xuewu Fu¹ , Hui Zhang¹, Kaihui Tang^{1,2}, Xun Wang¹ , Hui Zhang^{1,2}, Qianwen Deng^{1,2}, Leiming Zhang³, Kaiyun Liu⁴, Qingru Wu⁴, Shuxiao Wang⁴ , and Xinbin Feng^{1,2} 

¹State Key Laboratory of Environmental Geochemistry, Institute of Geochemistry, Chinese Academy of Sciences, Guiyang, China, ²University of Chinese Academy of Sciences, Beijing, China, ³Air Quality Research Division, Science and Technology Branch, Environment and Climate Change Canada, Toronto, ON, Canada, ⁴State Key Joint Laboratory of Environment Simulation and Pollution Control, School of Environment, Tsinghua University, Beijing, China

Abstract China is the largest contributor to the global total anthropogenic mercury (Hg) emissions. However, the trend in anthropogenic Hg emissions in recent years in China has not been effectively evaluated due to the lack of long-term atmospheric Hg observations. This study documents the changes in atmospheric gaseous elemental mercury (GEM) concentrations and isotopic compositions at Mt. Changbai (MCB) in northeastern China during 2015–2021 and Mt. Ailao (MAL) in southwestern China during 2017–2021, and explores the potential factors controlling these changes. GEM concentrations showed continuous declines from 2015 to 2021 ($-2.1 \pm 0.6\% \text{ yr}^{-1}$) at MCB and from 2017 to 2021 ($-4.0 \pm 1.4\% \text{ yr}^{-1}$) at MAL. Accompanied with these GEM declines are positive shifts in $\delta^{202}\text{Hg}$ (medians: from 0.42 to 0.46‰ at MCB and from 0.17 to 0.57‰ at MAL), and negative shifts in $\Delta^{199}\text{Hg}$ (medians: from -0.17‰ to -0.21‰ at MCB and from -0.10‰ to -0.17‰ at MAL) and $\Delta^{200}\text{Hg}$ values (medians: from -0.07‰ to -0.08‰ at MCB and from -0.03‰ to -0.05‰ at MAL) (at significant levels for $\Delta^{199}\text{Hg}$ at MCB and $\delta^{202}\text{Hg}$ and $\Delta^{199}\text{Hg}$ at MAL). These changes were mainly caused by the decreases in regional anthropogenic emissions in the study areas. Based on a ternary mixing model with $\Delta^{199}\text{Hg}$ and $\Delta^{200}\text{Hg}$ as input, we estimate decline rates of 5.8 ± 2.8 and $4.8 \pm 3.0\% \text{ yr}^{-1}$ for the regional anthropogenic GEM emissions in northeastern and southwestern China, respectively.

Plain Language Summary Long-term observations of atmospheric mercury (Hg) are important for evaluating the effectiveness of the Minamata Convention on Mercury. China is one of the largest anthropogenic atmospheric Hg emission regions in the world, and the temporal change in Chinese anthropogenic atmospheric Hg emissions plays an important role in global Hg cycling. However, long-term observations of atmospheric Hg in China are very limited, which makes it difficult to constrain the trend in atmospheric Hg concentrations in China and hampers our capability to evaluate the temporal changes in Chinese anthropogenic atmospheric Hg emissions. This study measures the gaseous elemental mercury (GEM) concentrations and isotopic compositions at two rural sites in China during 2015–2021 and 2017–2021, respectively. The results show rapid declines (-4.0% – $-2.1\% \text{ yr}^{-1}$) in GEM concentrations at the two sampling sites over the past 5–7 years, which are accompanied by systematically consistent increase of $\delta^{202}\text{Hg}$ and decrease of $\Delta^{199}\text{Hg}$ and $\Delta^{200}\text{Hg}$ values. Our observations indicate that the GEM declines are mainly driven by reduced anthropogenic emissions, and the reduction rates of regional anthropogenic emissions are estimated to be in the range of 4.8%–5.8% over the past 5–7 years.

1. Introduction

Gaseous elemental mercury (GEM or Hg(0)) plays a crucial role in the global mercury (Hg) cycling (Driscoll et al., 2013; Lindberg et al., 2007). Mercury released from anthropogenic and natural sources to the atmosphere is dominantly in the form of GEM (Lindberg et al., 2007). GEM generally has a much longer atmospheric residence time (~ 6 months) than gaseous oxidized mercury (GOM) and particulate bound mercury (PBM) and thus can be transported globally (Holmes et al., 2010; Shah et al., 2021). Once emitted into the atmosphere, GEM can undergo various physiochemical transformations to form GOM and PBM, which are readily deposited to earth surfaces via wet and dry deposition pathways (Driscoll et al., 2013). In addition, GEM could also

Writing – original draft: Xian Wu, Xuewu Fu

Writing – review & editing: Xuewu Fu, Hui Zhang, Kaihui Tang, Xun Wang, Hui Zhang, Qianwen Deng, Leiming Zhang, Kaiyun Liu, Qingru Wu, Shuxiao Wang, Xinbin Feng

be removed by the uptake by earth surfaces (ocean waters, organic soils) and vegetation (Jiskra et al., 2021; Obrist et al., 2017; Yuan et al., 2021; Zhu et al., 2022). Following deposition, mercury can be converted to methylmercury in aquatic ecosystems (Driscoll et al., 2013), posing severe health risks to human and wildlife health.

Since the industrialization, GEM concentrations in air have been increasing on the global scale due to increasing primary anthropogenic Hg emissions as well as contributions from re-emission of previously deposited Hg originated from anthropogenic sources (Amos et al., 2013; Enrico et al., 2017; Streets et al., 2019b). GEM concentrations started declining after 1990's in North America and Europe owing to the implementation of air pollution control measures, which reduced anthropogenic Hg emissions in these regions (Slemr et al., 2003; Streets et al., 2019b; Y. X. Zhang et al., 2016). However, GEM concentrations in developing countries remain high or are even increasing in the recent decades due to increasing anthropogenic Hg emissions in these regions, which may offset the effort of emission reductions achieved in developed regions in terms of global Hg budget (Streets et al., 2019a; Y. X. Zhang et al., 2016). Levels of GEM in air generally tend to decrease with decreasing anthropogenic Hg emissions, and thus a long-term monitoring of GEM is needed for tracking the trends of GEM and effectiveness of emission reduction policies (Amos et al., 2013; K. Y. Liu et al., 2019; Y. X. Zhang et al., 2016).

China is the largest contributor (~25% in 2015) to the global total anthropogenic Hg emissions (AMAP/UNEP, 2019). Anthropogenic Hg emissions in China have increased for several decades before starting to decrease in the most recent decade (K. Y. Liu et al., 2019; Wu et al., 2016). The recent decline is yet to be evaluated by long-term monitored GEM data (K. Y. Liu et al., 2019). Existing studies have reported the trends in GEM concentrations at three sites in eastern China covering a few (≤ 4) years (Qin et al., 2020; Tang et al., 2018; Wu et al., 2020). Analysis of these data using multiple source identification methods, including trajectory-based source identification, positive matrix factorization, and statistical models, helps to understand the mechanisms controlling GEM concentrations. However, it remains a challenge to establish the direct links between the changing GEM concentrations and various emission sources (e.g., anthropogenic sources and surface emissions) and atmospheric processes because of a lack of direct and convincing tracers of these influencing factors.

Mercury stable isotopes can be potentially used for tracking the sources and biogeochemical processes of Hg in natural environments. Mercury isotopes can undergo mass dependent fractionation (MDF, $\delta^{202}\text{Hg}$ signatures) and odd- and even-mass independent fractionation (MIF, $\Delta^{199}\text{Hg}$ and $\Delta^{200}\text{Hg}$ signatures) during environmental transformations (Blum et al., 2014). Recent studies on the isotope composition of anthropogenic GEM emissions showed moderate negative $\delta^{202}\text{Hg}$ (e.g., -0.58‰) and near-zero $\Delta^{199}\text{Hg}$ and $\Delta^{200}\text{Hg}$ signatures (R. Y. Sun et al., 2016, 2019), which differ appreciably from those of land surfaces emissions (e.g., $\delta^{202}\text{Hg} = -1.13\text{‰}$; $\Delta^{199}\text{Hg} = -0.13\text{‰}$; $\Delta^{200}\text{Hg} = 0.02\text{‰}$) and background atmospheric pools (e.g., $\delta^{202}\text{Hg} = 0.43\text{‰}$; $\Delta^{199}\text{Hg} = -0.20\text{‰}$; $\Delta^{200}\text{Hg} = -0.05\text{‰}$) (Jiskra et al., 2021; Yuan et al., 2019, 2021; Zhu et al., 2022). The different isotopic signatures for different Hg sources provide a basis for identifying sources of atmospheric GEM making use of Hg stable isotopes. Measurements of Hg isotopic compositions and trends in environmental reservoirs are helpful for better understanding the impact of anthropogenic emissions on Hg biogeochemical cycling and evaluating the effectiveness of emission control measures under the Minamata Convention (Kwon et al., 2020). Previous studies observed coherent changes in sediment Hg isotopic compositions with the increase of anthropogenic emissions since industrialization, indicating essential response of atmospheric Hg isotopic compositions to the anthropogenic drivers (Lepak et al., 2020). To date, however, studies on the temporal changes in atmospheric Hg isotopic compositions as well as their potential drivers are still lacking.

In the present study, we first analyzed GEM concentrations that were continuously measured at the remote Mt. Changbai (MCB) in northeastern China during April 2015 and November 2021 and Mt. Ailao (MAL) in southwestern China during January 2017 and November 2021. We then analyzed isotopic compositions of GEM that were measured in the first and last year of the observation period at both sites. The objectives of this study are to: (a) document the temporal trends in atmospheric GEM at remote sites in China; (b) investigate the response of GEM isotopic compositions to the changes of GEM concentrations; and (c) explore the factors controlling the changes in GEM concentrations and isotopic compositions and estimate the changes in anthropogenic Hg emissions using Hg stable isotopes.

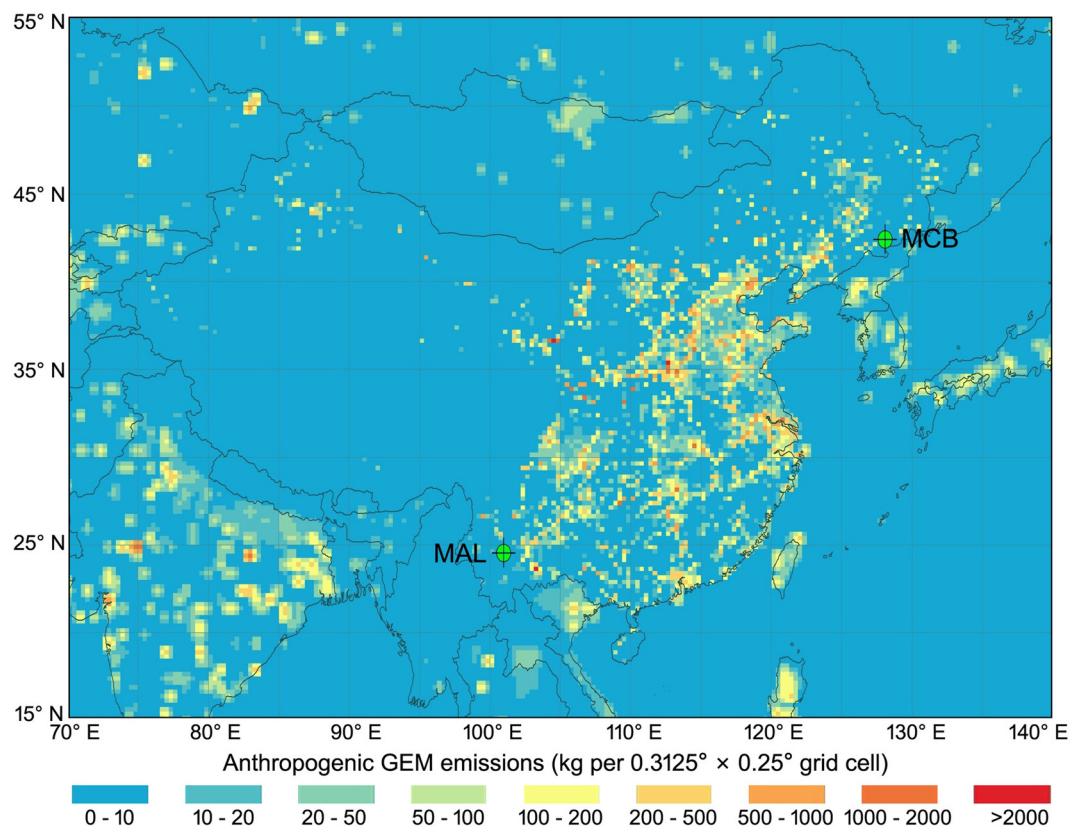


Figure 1. Location of Mt. Changbai and Mt. Ailao and gridded anthropogenic gaseous elemental mercury emissions in China in 2013 and outside China in 2010 (AMAP/UNEP, 2013; K. Y. Liu et al., 2019).

2. Materials and Methods

2.1. Sampling Sites

Observations of GEM concentrations and isotopic compositions were conducted at Mt. Changbai (MCB, 128.113°E, 42.400°N, 741 m above sea level (a.s.l.)) and Mt. Ailao (MAL, 101.020°E, 24.533°N, 2450 m a.s.l.) forest sites in northeastern and southwestern China, respectively. These two sites are regional background sites because there were no strong point Hg sources within 50 km in radius (Figure 1). Continuous monitoring of GEM started from October 2008 at MCB and from May 2011 at MAL. These two sampling sites were operated as master observational stations in the Global Mercury Observation System (GMOS) during 2011–2015 (Sprovieri et al., 2016). Additional descriptions of the sampling sites can be found in a previous study (Fu et al., 2019).

2.2. Continuous GEM Measurements

GEM concentrations were continuously measured at an interval of 5 min using Tekran 2537 mercury vapor analyzers. The analyzers are designed to measure GEM at sub-ng m⁻³ levels based on collection of GEM onto dual gold cartridges, followed by thermal desorption and detections using Cold Vapor Atomic Fluorescence Spectrometry (CVAFS). The data quality was controlled by internal permeation source calibrations every 47 hr at MCB and 71 hr at MAL, which were also routinely (months to a year) checked using external Hg(0) vapor sources. The operations and maintenance of the analyzers followed the GMOS standard operating procedures (Sprovieri et al., 2016). In the present study, GEM concentration data at MCB from April 2015 to November 2021 and at MAL from January 2017 to November 2021 are presented considering that the starting and ending months were also covered by GEM isotope observations at the same sites. At MCB and MAL, GOM on average was less than 1% of GEM (Fu, Zhu, et al., 2016; H. Zhang et al., 2016), and thus the observations of concentrations and isotopic compositions are fully assigned to GEM in this study.

2.3. Sampling, Processing, and Analysis of GEM Isotopic Compositions

Isotopic compositions of GEM at MCB during April 2015 and April 2016 and at MAL during January and December 2017 were measured in our previous study (Fu et al., 2019), and the same method as described in the previous study was also used to measure the GEM isotope composition at MCB and MAL during November 2020 and November 2021. Briefly, ambient GEM was continuously collected for 10 days using CLC (chlorine-impregnated activated carbon, 0.5 g) traps at a flow rate of 2.0–2.5 L min⁻¹ (Fu et al., 2014). GEM collected onto CLC traps was thermally desorbed in a Hg-free argon gas flow and subsequently trapped by mixed acid trapping solutions (2HNO₃/1HCl, v/v, 5 mL) (K. Li et al., 2019). The trapping solutions containing Hg were kept at 2–4°C in a refrigerator before analysis for concentrations and isotope ratios. Blanks of CLC traps were measured, which showed a mean blank value of 0.17 ± 0.09 ng (1sd, n = 10), accounting for less than 1% of the total mass of GEM collected by CLC. Recoveries of CLC traps for GEM sampling were tested by injections of Hg(0) vapor, which showed values ranging from 86.3% to 108.1% (mean = 98.5 ± 5.8%, 1sd, n = 10). GEM concentration of each sample was calculated based on the detection of Hg concentration in trapping solution using CVAFS and sampling volume, which are in agreement with the concentrations measured by Tekran 2537 (GEM_{CLC}/GEM_{Tekran} ranged from 88.9% to 126.6% with a mean of 106.1 ± 10.8% at MCB and from 77.2% to 128.2% with a mean of 97.9 ± 11.5% at MAL).

Isotope ratios of Hg in trapping solutions were measured using cold vapor-multicollector inductively coupled plasma mass spectrometry (CV-MC-ICPMS, Nu Instruments, U.K.) following a previous study (Fu et al., 2019). MDF signatures are reported in delta notation (δ, ‰) and calculated as follows (Blum & Bergquist, 2007):

$$\delta^{xxx}\text{Hg} = \left[\left(\frac{^{xxx}\text{Hg}/^{198}\text{Hg}}{^{xxx}\text{Hg}/^{198}\text{Hg}} \right)_{\text{sample}} / \left(\frac{^{xxx}\text{Hg}/^{198}\text{Hg}}{^{xxx}\text{Hg}/^{198}\text{Hg}} \right)_{\text{NIST 3133}} - 1 \right] \times 1000\text{‰} \quad (1)$$

where ^{xxx}Hg represents the mercury stable isotopes (¹⁹⁹Hg, ²⁰⁰Hg, ²⁰¹Hg, ²⁰²Hg, and ²⁰⁴Hg). NIST 3133 refers to bracketing NIST (National Institute of Standards & Technology) SRM (Standard Reference Material) 3133 mercury standard solution, of which the mercury isotope ratios were measured before and after the sample collection to correct the mass bias of MC-ICPMS. MIF signatures (Δ¹⁹⁹Hg, Δ²⁰⁰Hg, Δ²⁰¹Hg, and Δ²⁰⁴Hg) were calculated based on the Kinetic MDF law as follows (Blum & Bergquist, 2007):

$$\Delta^{xxx}\text{Hg} (\text{‰}) = \delta^{xxx}\text{Hg} - (\beta^{xxx} \times \delta^{202}\text{Hg}) \quad (2)$$

where β^{xxx} is 0.252, 0.5024, 0.752, and 1.493 for ¹⁹⁹Hg, ²⁰⁰Hg, ²⁰¹Hg, and ²⁰⁴Hg, respectively.

Isotopic compositions of NIST RM (Reference material) 8610 (UM-Almaden Mono-Elemental Secondary Standard) and CRM (Certified Reference Material) BCR (Community Bureau of Reference) 482 Lichen were repeatedly measured (every 2–4 samples) to quantify the analytical uncertainties of GEM isotopic compositions, which are in agreement with the reference values and previously reported values (Table S1 in Supporting Information S1). To ensure the comparability of GEM isotopic compositions between different years, Hg(0) vapor with known isotopic compositions extracted from NIST RM 8610 solutions were added into the CLC traps at the typical sampling flow rate, similar to those conducted in our previous observations (Fu et al., 2019). The average δ²⁰²Hg, Δ¹⁹⁹Hg, and Δ²⁰⁰Hg values of the addition tests were 0.50 ± 0.13‰, -0.03 ± 0.04‰, and 0.00 ± 0.05‰ (2sd, n = 7), respectively, which are consistent with the reference values (Table S1 in Supporting Information S1). In this study, the larger 2sd value of either repeated measurements of NIST RM 8610 during the whole analytical sessions or the internal repeated measurements of an individual GEM sample is used to report the analytical uncertainty of GEM isotopic compositions.

2.4. Ancillary Parameters and Statistical Method

72-hr air mass backward trajectories ended at MCB and MAL at a height of 100 m above ground level (a.g.l.) were calculated every 6 hr using a GIS trajectory analysis tool (TrajStat) based on GDAS (Global Data Assimilation System) gridded meteorological data from the U.S. National Oceanic and Atmospheric Administration (NOAA) (Y. Q. Wang et al., 2009). Potential source regions were identified using a Concentration-Weighted Trajectory (CWT) receptor-based model (Text S1 in Supporting Information S1) (Cheng et al., 2013; H. Zhang et al., 2016). Mean cumulative anthropogenic GEM emissions (∑anthropogenic emissions, in kg 0.3125° × 0.25° grid⁻¹ h⁻¹), which represent the exposure to anthropogenic GEM emissions during the transport of air masses within boundary layer (e.g., <1,000 m a.g.l.) during the preceding 72 hr, were calculated based on the simulated backward

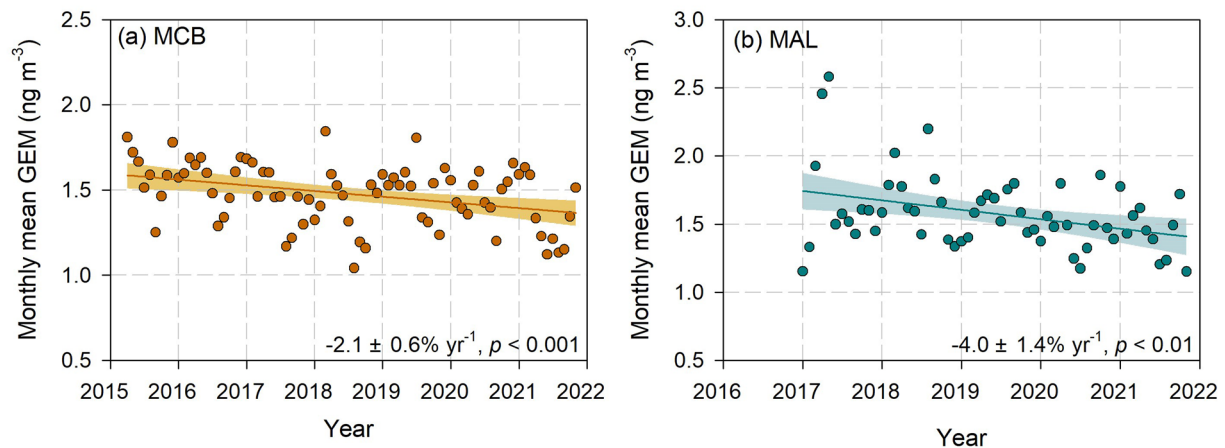


Figure 2. Monthly mean gaseous elemental mercury (GEM) concentrations at Mt. Changbai from April 2015 to November 2021 (a) and Mt. Ailao from January 2017 to November 2021 (b). Line indicates the trend in GEM concentrations and shaded area represents the 95% confidence level of the trend.

trajectories and gridded anthropogenic GEM emissions ($0.3125^{\circ} \times 0.25^{\circ}$ grid, emissions in China and outside China are from K. Y. Liu et al. (2019) and AMAP/UNEP (2013), respectively) (Text S2 in Supporting Information S1; Figure 1). K. Y. Liu et al. (2019) revealed that anthropogenic Hg emissions in China were decreasing during 2013–2017, and the decreasing rates were broadly similar over different regions across China (Figure S1 in Supporting Information S1). Therefore, using emission inventory in 2013 would overestimate the Σ anthropogenic emissions during the study periods, but is not expected to confound the interpretation of the impact of anthropogenic emissions on the observed GEM concentrations. NDVI (Normalized Difference Vegetation Index) at local scale (e.g., 0.5×0.5 grid) was scaled from the global gridded NDVI data (NOAA Earth Observations) to investigate the changes in vegetation activities. Temporal trends in GEM concentrations and ancillary parameters were analyzed using the IBM SPSS Statistic 23 (ANOVA, method: all requested variables entered).

3. Results and Discussion

3.1. Trends in GEM Concentrations and Isotope Compositions

Monthly mean and median GEM concentrations at MCB between April 2015 and November 2021 and at MAL between January 2017 and November 2021 are shown in Figure 2; Figure S2 in Supporting Information S1, respectively. The average (± 1 sd) GEM concentrations at MCB and MAL during the whole study periods were 1.48 ± 0.18 and 1.58 ± 0.28 ng m^{-3} , respectively. These values are slightly higher than the mean GEM concentrations obtained at forest sites in Europe (Schmücke, Schauinsland, and Pallas) and North America (Piney Reservoir, Huntington Wildlife, Kejimikujik National Park, and Athens Super Site) during the period of 2015–2020 (1.18 – 1.52 ng m^{-3} with an overall mean of 1.34 ng m^{-3} , $n = 7$) (NADP, 2022; Tørseth et al., 2012). Linear Regression analysis on the continuous GEM data showed statistically significant declines at MCB during 2015–2021 ($-2.1 \pm 0.6\% \text{ yr}^{-1}$, $p < 0.001$) and MAL during 2017–2021 ($-4.0 \pm 1.4\% \text{ yr}^{-1}$, $p < 0.01$). These decreasing rates are comparable with the decline (-3.0%) of GEM concentrations in mainland China during 2013–2017 simulated using a GEOS-Chem model (K. Y. Liu et al., 2019), but considerably lower than those (-22.3% – $-8.0\% \text{ yr}^{-1}$) observed at sites close to major anthropogenic source regions in eastern and northern China (e.g., Chongming Island during 2014–2016, Dianshan Lake during 2015–2018, and Beijing during 2015–2018) (Qin et al., 2020; Tang et al., 2018; Wu et al., 2020).

Comparing the 2 years with GEM isotope observations, that is, April 2015 to April 2016 versus November 2020 to November 2021 at MCB (months = 12), and January to December 2017 versus November 2020 to November 2021 at MAL (months = 12), annual mean GEM concentrations decreased from 1.57 ± 0.16 to 1.38 ± 0.21 ng m^{-3} ($2.2 \pm 0.8\% \text{ yr}^{-1}$) at MCB at a significant level (Two-independent sample t test, $p < 0.05$) and from 1.68 ± 0.32 to 1.47 ± 0.17 ng m^{-3} ($3.2 \pm 2.0\% \text{ yr}^{-1}$) at MAL at an insignificant level (Two-independent sample t test, $p = 0.15$) (Figure S3 in Supporting Information S1), in agreement with the trend determined from the year to year continuous GEM observations. Such a decline in GEM concentrations was accompanied by

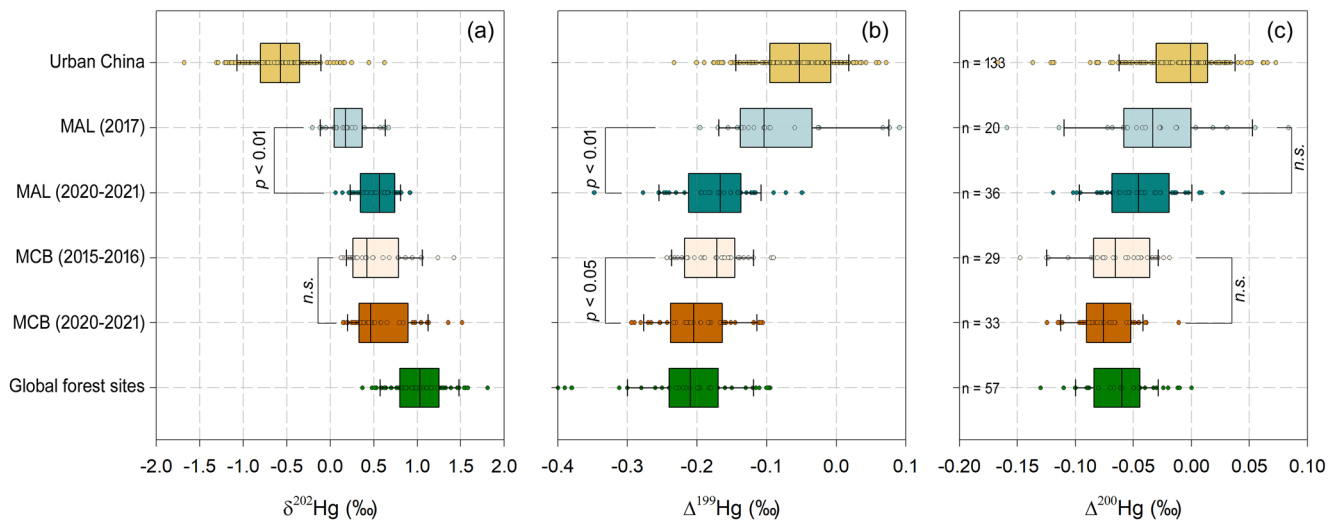


Figure 3. Statistical summary of the gaseous elemental mercury (GEM) isotopic compositions ((a) $\delta^{202}\text{Hg}$, (b) $\Delta^{199}\text{Hg}$, and (c) $\Delta^{200}\text{Hg}$) at Mt. Changbai (April 2015 to April 2016 (Fu et al., 2019) versus November 2020 to November 2021) and MAL (January to December 2017 (Fu et al., 2019) versus November 2020 to November 2021). Isotopic compositions of GEM in urban China and global forests are from literature (Demers et al., 2013; Enrico et al., 2016; Fu, Liu, et al., 2021; Kurz et al., 2020; Yu et al., 2022). Left whiskers, boxes, lines within boxes, and right whiskers indicate the $-1.5 * \text{IQR}$, interquartile range, median, and $+1.5 * \text{IQR}$, respectively, of the grouped observations. Dots are the isotopic compositions of individual GEM sample.

increasing $\delta^{202}\text{Hg}$ and decreasing $\Delta^{199}\text{Hg}$ and $\Delta^{200}\text{Hg}$ values (Figure 3). At MCB, the median $\delta^{202}\text{Hg}$, $\Delta^{199}\text{Hg}$, and $\Delta^{200}\text{Hg}$ values of GEM during November 2020 and November 2021 were 0.46‰ (interquartile range (IQR): $0.34\text{--}0.84\text{‰}$), -0.21‰ (IQR: $-0.23\text{--}-0.17\text{‰}$), and -0.08‰ (IQR: $-0.09\text{--}-0.05\text{‰}$) ($n = 33$), respectively, which were 0.04‰ higher and 0.04 and 0.01‰ lower than the corresponding median values ($\delta^{202}\text{Hg} = 0.42$ (IQR: $0.26\text{--}0.78\text{‰}$), $\Delta^{199}\text{Hg} = -0.17$ (IQR: $-0.21\text{--}-0.15\text{‰}$), and $\Delta^{200}\text{Hg} = -0.07$ (IQR: $-0.08\text{--}-0.04\text{‰}$), $n = 29$) during April 2015 and April 2016, respectively (Figure 3; Figure S3 and Table S2 in Supporting Information S1) (Fu et al., 2019). A similar trend in GEM isotopic compositions was also observed at MAL, with the median $\delta^{202}\text{Hg}$ (0.57‰ , IQR: $0.36\text{--}0.74\text{‰}$), $\Delta^{199}\text{Hg}$ (-0.17‰ , IQR: $-0.20\text{--}-0.14\text{‰}$), and $\Delta^{200}\text{Hg}$ (-0.05‰ , IQR: $-0.07\text{--}-0.02\text{‰}$) during November 2020 and November 2021 ($n = 36$) being 0.40‰ higher and 0.07 and 0.02‰ lower than the corresponding median values ($\delta^{202}\text{Hg} = 0.17\text{‰}$, IQR: $0.05\text{--}0.31\text{‰}$; $\Delta^{199}\text{Hg} = -0.10\text{‰}$, IQR: $-0.14\text{--}-0.05\text{‰}$; and $\Delta^{200}\text{Hg} = -0.03$, IQR: $-0.06\text{--}-0.01\text{‰}$, $n = 20$) during January and December 2017, respectively (Figure 3; Figure S3 and Table S2 in Supporting Information S1). The changes in GEM isotopic compositions between the two individual years are statistically significant (Two-independent sample t test) for $\Delta^{199}\text{Hg}$ at MCB ($p < 0.05$) and $\delta^{202}\text{Hg}$ and $\Delta^{199}\text{Hg}$ at MAL ($p < 0.01$ for both), whereas they are not statistically significant for $\delta^{202}\text{Hg}$ and $\Delta^{200}\text{Hg}$ at MCB and $\Delta^{200}\text{Hg}$ at MAL ($p > 0.05$ for all) (Figure 3).

GEM $\delta^{202}\text{Hg}$ values at MCB and at MAL during November 2020 to November 2021 showed a clear seasonal variation with higher GEM $\delta^{202}\text{Hg}$ values observed in summer and early autumn (Figure S3 in Supporting Information S1), which were significantly correlated with NDVI (ANOVA, $r^2 = 0.54\text{--}0.71$, $p < 0.01$ for both), indicating the important role of vegetation activity on seasonal variation in GEM $\delta^{202}\text{Hg}$. Such a seasonal pattern was also observed at MCB during April 2015 and April 2016, but was not observed at MAL during January and December 2017 (Figure S3 in Supporting Information S1), which was likely obscured by the strong seasonal changes in the transport of anthropogenic emissions (Fu et al., 2019). Generally, GEM isotopic compositions at MCB and MAL fell in the range of those observed at urban sites in China and other global background forest sites (Figure 3). GEM $\delta^{202}\text{Hg}$ values at MCB and MAL were much higher than those observed at urban sites in China with strong anthropogenic emissions (site-specific median, $\delta^{202}\text{Hg} = -1.05\text{--}-0.07\text{‰}$, $n = 11$), and much lower than those at other global background forest sites (site-specific median, $\delta^{202}\text{Hg} = 0.70\text{--}1.20\text{‰}$, $n = 4$). GEM $\Delta^{199}\text{Hg}$ and $\Delta^{200}\text{Hg}$ values at MCB and MAL were much lower than those in urban areas (site-specific median, $\Delta^{199}\text{Hg} = -0.12\text{--}-0.01\text{‰}$, $\Delta^{200}\text{Hg} = -0.03\text{--}0.02\text{‰}$, $n = 11$), and slightly higher/similar as compared with those at other global background forests (site-specific median, $\Delta^{199}\text{Hg} = -0.25\text{--}-0.19\text{‰}$, $\Delta^{200}\text{Hg} = -0.10\text{--}-0.05\text{‰}$, $n = 4$) (Demers et al., 2013; Enrico et al., 2016; Fu, Liu, et al., 2021; Kurz et al., 2020; Yu et al., 2022). Overall, isotopic signatures of GEM at both MCB and MAL differed more significantly from those at Chinese urban sites

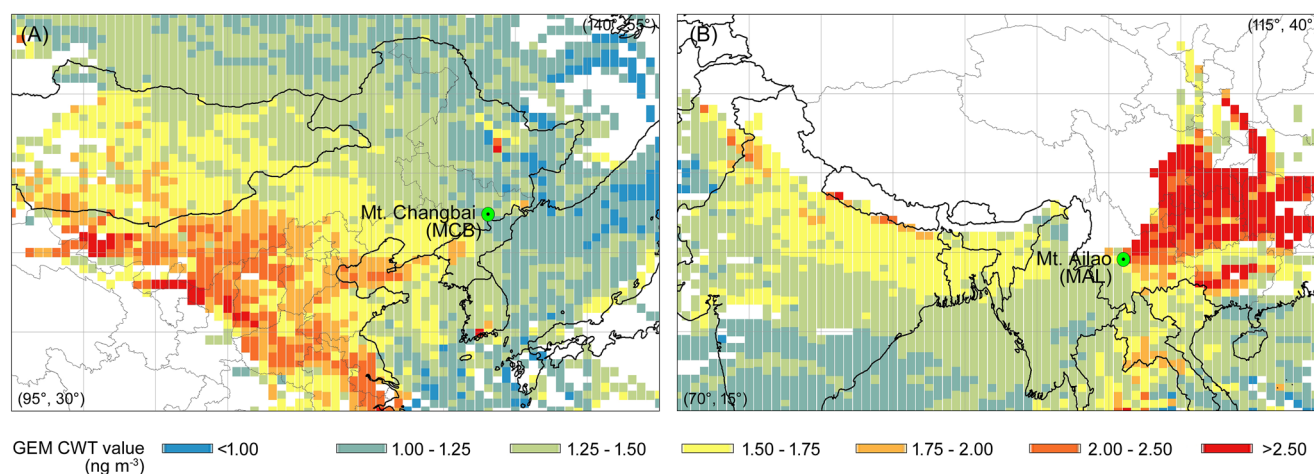


Figure 4. Potential source regions identified using Concentration-Weighted Trajectory model at Mt. Changbai (a) and Mt. Ailao (b) during November 2020 and November 2021.

during 2020–2021 than the preceding 4–6 years, indicating a relatively weaker impact of anthropogenic emissions during 2020–2021.

3.2. Causes of the Changes in GEM Concentrations and Isotope Compositions

Changes in surface GEM concentrations and isotopic compositions could be affected by anthropogenic emissions, terrestrial surface emissions, global background atmospheric pool, vegetation activities, and atmospheric oxidation processes (Fu et al., 2019; Fu, Jiskra, et al., 2021; Jiskra et al., 2018; Lei et al., 2014; Slemr et al., 2011; Wu et al., 2020; Y. X. Zhang et al., 2016). In the present study, we analyzed the source regions using a CWT model and found the major source regions of GEM at MCB were in northern and eastern China, while those at MAL were in southwestern China (Figure 4). The gridded GEM CWT values at MCB and MAL were significantly positively correlated with gridded anthropogenic GEM emissions ($r^2 = 0.66\text{--}0.78$, $p < 0.01$ for both sites, Text S1 and Figure S4 in Supporting Information S1) (AMAP/UNEP, 2013; K. Y. Liu et al., 2019), indicating anthropogenic emissions were an important factor controlling the variations in GEM concentrations at MCB and MAL. Due to the air pollutant emission control measures implemented since a decade ago, anthropogenic Hg emissions in China are expected to decrease in recent years (K. Y. Liu et al., 2019). We therefore tried to verify whether the declines of GEM concentrations at MCB and MAL were mainly driven by decreases in anthropogenic emissions.

In China, cement production, coal combustion, and non-ferrous metal smelting are the dominant source sectors of anthropogenic Hg emissions (K. Y. Liu et al., 2019), and the Hg isotope signatures of source materials ($n = 182$) for these source sectors are compiled and shown in Table S3 in Supporting Information S1 (Fan et al., 2021; Shen et al., 2019; Yin et al., 2014, 2016). Based on the relative contributions of these source sectors to the total anthropogenic GEM emissions in China in 2017 (K. Y. Liu et al., 2019), we estimated that median $\Delta^{199}\text{Hg}$ and $\Delta^{200}\text{Hg}$ of GEM emitted from Chinese anthropogenic sources are 0.02‰ (IQR: $-0.01\text{--}0.06\text{‰}$) and 0.02‰ (IQR: $0.00\text{--}0.03\text{‰}$), respectively ($\delta^{202}\text{Hg}$ was not calculated due to the MDF of Hg isotopes during emission processes). These values are in agreement with the isotope signatures estimated for global anthropogenic GEM emissions ($\delta^{202}\text{Hg} = -0.58\text{‰}$, $\Delta^{199}\text{Hg} = -0.02\text{‰}$, $\Delta^{200}\text{Hg} = 0.00\text{‰}$) (R. Y. Sun et al., 2019), but much more positive as compared with the GEM mainly impacted by free tropospheric air masses ($\delta^{202}\text{Hg} = 0.36\text{‰}$ (median, IQR: $0.09\text{--}0.47\text{‰}$), $\Delta^{199}\text{Hg} = -0.28\text{‰}$ (median, IQR: $-0.31\text{--}0.24\text{‰}$), $\Delta^{200}\text{Hg} = -0.11\text{‰}$ (median, IQR: $-0.14\text{--}0.07\text{‰}$), $n = 20$) (Figure 5; Table S3 in Supporting Information S1) (Fu, Jiskra, et al., 2021; Kurz et al., 2020; Nguyen et al., 2021). Thus, a decrease in anthropogenic emissions in China has the potential to lower the relative contributions of anthropogenic emissions, subsequently shifting the GEM isotopic compositions toward higher $\delta^{202}\text{Hg}$ and lower $\Delta^{199}\text{Hg}$ and $\Delta^{200}\text{Hg}$ values as observed in this study (Figure 5).

In addition to the decreases in anthropogenic emissions, changes in transport patterns of anthropogenic emissions may also be important for the shifting of the GEM isotopic compositions. Less anthropogenic GEM emissions transported to MCB and MAL due to changing regional atmospheric transport patterns would have similar

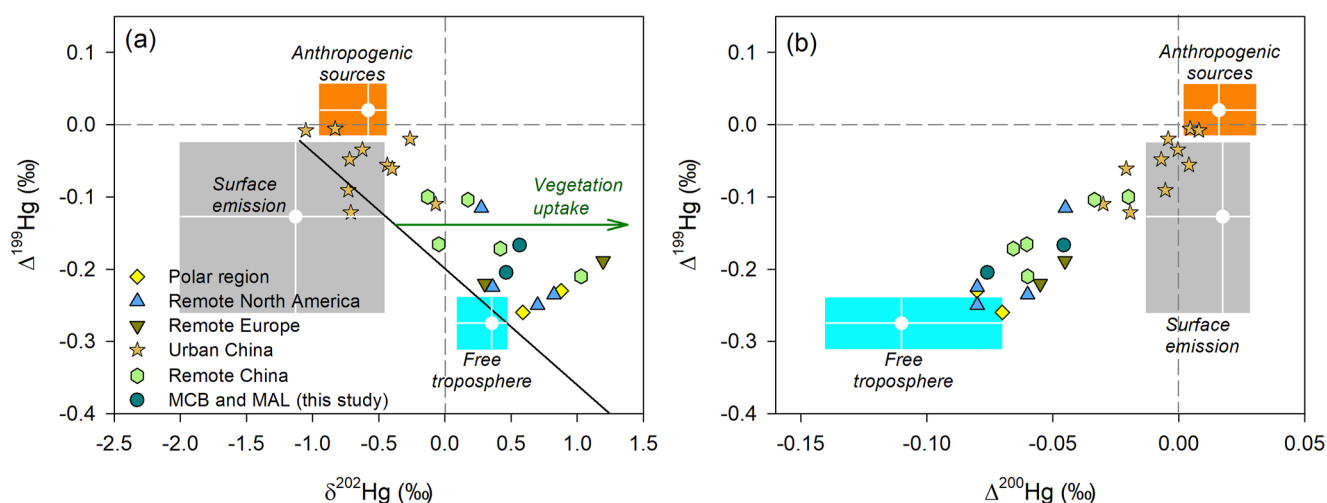


Figure 5. Site-specific median gaseous elemental mercury (GEM) isotopic compositions at global surface sites ($n = 25$, Table S4 in Supporting Information S1) and statistical summary of the isotopic compositions of GEM emissions from anthropogenic sources and land surfaces, and background free tropospheric GEM pool (a) $\delta^{202}\text{Hg}$ vs. $\Delta^{199}\text{Hg}$ and (b) $\Delta^{200}\text{Hg}$ vs. $\Delta^{199}\text{Hg}$). Data are from this study and the following literature: anthropogenic GEM emissions (Fan et al., 2021; Shen et al., 2019; R. Y. Sun et al., 2016; Yin et al., 2014, 2016), land surface GEM emissions (Yuan et al., 2019, 2021; Zhu et al., 2022), background free tropospheric GEM pool (Fu, Jiskra, et al., 2021; Kurz et al., 2020; Nguyen et al., 2021), and atmospheric GEM at other surface sites (Demers et al., 2015; Enrico et al., 2016; Fu et al., 2018, 2019; Fu, Jiskra, et al., 2021; Gratz et al., 2010; Jiskra et al., 2019; Kurz et al., 2020; Nguyen et al., 2021; Obrist et al., 2017; Yu et al., 2021, 2022). White circles within the shaded boxes indicate the median $\delta^{202}\text{Hg}$, $\Delta^{199}\text{Hg}$, and $\Delta^{200}\text{Hg}$ estimated for anthropogenic emissions, land surface emissions, and background free tropospheric pool, and the shaded boxes indicate the interquartile range of estimated isotopic compositions.

impact on the changes in surface GEM concentrations and isotopic compositions as to those caused by reduced anthropogenic emissions. We calculated \sum anthropogenic GEM emissions to evaluate whether the changes in GEM concentrations and isotopic compositions were due to less exposure of air masses to anthropogenic emissions (Text S2 in Supporting Information S1). At MCB, yearly mean \sum anthropogenic emissions show a slightly increase during 2015–2021 ($0.4 \pm 1.0\% \text{ yr}^{-1}$, $p = 0.57$), while yearly mean \sum anthropogenic emissions at MAL show a considerable decline ($\sim 32\%$) from 2018 to 2019 but turn to increase during 2019–2021 ($6.1 \pm 2.9\% \text{ yr}^{-1}$, Figure S5 in Supporting Information S1). These \sum anthropogenic emissions trends are not consistent with those of GEM concentrations. Thus, the interannual variations in the transport of anthropogenic emissions likely played a minor role in the temporal changes of GEM concentrations at these two sites. The annual mean \sum anthropogenic emission at MAL during November 2020 and November 2021 was 17% lower than that during January and December 2017, which may partly explain the increase of $\delta^{202}\text{Hg}$ and decrease of GEM concentrations and $\Delta^{199}\text{Hg}$ at this site. In contrast, the changes in the mean \sum anthropogenic emissions at MCB from April 2015–April 2016 to November 2020–November 2021 were extremely small (increased by 2%), which was not likely the main cause of the significant changes in GEM concentrations and $\Delta^{199}\text{Hg}$ at MCB.

GEM emissions from terrestrial surfaces (mainly soils) are also an important factor controlling the GEM levels in China (X. Wang et al., 2016). Isotopic compositions of GEM net emissions from terrestrial surfaces were recently investigated, which showed lower $\delta^{202}\text{Hg}$ (median: -1.13‰ , IQR: -2.00‰ – -0.47‰) and $\Delta^{199}\text{Hg}$ (median: -0.13‰ , IQR: -0.26‰ – -0.02‰), and similar $\Delta^{200}\text{Hg}$ (median: 0.02‰ , IQR: -0.01‰ – 0.03‰) as compared with those of anthropogenic emissions (Figure 5; Table S3 in Supporting Information S1) (Yuan et al., 2019, 2021; Zhu et al., 2022). Thus, decreasing surface emissions could also lead to decreases in GEM concentrations and $\Delta^{200}\text{Hg}$ and increases in $\delta^{202}\text{Hg}$ values, but would cause insignificant $\Delta^{199}\text{Hg}$ shift because the GEM $\Delta^{199}\text{Hg}$ at MCB and MAL in earlier years were close to that emitted from land surfaces. Surface GEM emissions are mainly controlled by substrates Hg concentrations, solar radiation, and temperature (Agnan et al., 2016). Regional net radiation and surface temperatures at MCB and MAL were relatively constant during the study period (Figures S6 and S7 in Supporting Information S1), implying relatively stable soil Hg emissions considering that the large mass and long lifetime of Hg in soil pool (Smith-Downey et al., 2010; W. B. Sun et al., 2022). Decreases in anthropogenic emissions would reduce atmospheric input to soil Hg through atmospheric deposition, which in turn affects surface GEM emissions due to re-emission processes. However, the decreasing rate should be low (e.g., $\sim 0.24\% \text{ yr}^{-1}$ under zero anthropogenic emissions scenario) according to modeling studies (Amos et al., 2013; Smith-Downey et al., 2010), which is insufficient to dominate the significant declines in GEM concentrations.

Observations of nighttime GEM concentrations at Mauna Loa, USA (dominated by katabatic wind) showed an insignificant weak decline ($-0.26 \pm 0.76\% \text{ yr}^{-1}$, $p = 0.74$) during 2015–2020 (Figure S8 in Supporting Information S1) (NADP, 2022), which is much lower than the trends observed at MCB and MAL ($-4.0\% \text{--} -2.1\% \text{ yr}^{-1}$). GEM in the free troposphere is generally characterized by much higher $\delta^{202}\text{Hg}$ and much lower $\Delta^{199}\text{Hg}$ and $\Delta^{200}\text{Hg}$ relative to those from anthropogenic and surface emissions (Figure 5; Table S3 in Supporting Information S1) (Fan et al., 2021; Fu, Jiskra, et al., 2021; Kurz et al., 2020; Nguyen et al., 2021; Shen et al., 2019; R. Y. Sun et al., 2016; Yin et al., 2014, 2016; Yuan et al., 2021; Zhu et al., 2022). If the declines at MCB and MAL were mainly caused by a decline in the global background GEM pool, a decrease of $\delta^{202}\text{Hg}$ and increases of $\Delta^{199}\text{Hg}$ and $\Delta^{200}\text{Hg}$ at MCB and MAL would be anticipated because the relative contributions of anthropogenic and surface emissions to surface GEM would increase. This is in contrast with the changes in GEM isotopic compositions, suggesting a minor role of global background atmospheric pool in the observed GEM trend.

Exchange of GEM between foliar and atmosphere would lead to a positive shift in $\delta^{202}\text{Hg}$ due to foliar uptake and a small negative shift in $\Delta^{199}\text{Hg}$ due to re-emission of Hg from foliage, and this explains well the significant positive $\delta^{202}\text{Hg}$ values observed at global forest sites (Figures 3 and 5) (Demers et al., 2013; Fu et al., 2019; Yuan et al., 2019). According to a previous study at MCB, a 100% increase of NDVI (representing vegetation activity) would result in a decline of $\sim 15\%$ in GEM concentrations, a $+0.50\%$ shift in $\delta^{202}\text{Hg}$, and a $+0.05\%$ shift in $\Delta^{199}\text{Hg}$ (Fu et al., 2019). However, the interannual changes in NDVI at MCB and MAL were extremely small (from 0.54 to 0.57 at MCB during 2015–2021 and from 0.71 to 0.72 at MAL during 2017–2021, Figure S9 in Supporting Information S1), which unlikely cause significant temporal changes in GEM concentrations and isotope compositions.

Oxidation of GEM plays an important role in the global GEM cycling (Holmes et al., 2010; Selin et al., 2007), however, its roles on the long-term trends in GEM is still not well understood. Annual mean GEM concentrations at MCB ($5.4 \pm 6.4 \text{ pg m}^{-3}$) and MAL ($2.2 \pm 2.3 \text{ pg m}^{-3}$) were much lower than those observed at other high-altitude sites in the Northern Hemisphere (means: $14.0\text{--}43 \text{ pg m}^{-3}$) (Fain et al., 2009; Fu, Maruszczak, et al., 2016; C. Liu et al., 2022; Sheu et al., 2010; Swartzendruber et al., 2006; H. Zhang et al., 2016), indicating the oxidation of GEM is relatively slow at MCB and MAL. Recent global atmospheric Hg modeling proposed that GEM is oxidized to Hg(II) via a two-step oxidation, with atomic bromine (Br) and OH as the main oxidants during the first step (Holmes et al., 2010; Saiz-Lopez et al., 2020; Shah et al., 2021). Concentrations of reactive bromine and OH were not measured at our stations, but modeling studies proposed that the levels of reactive bromine and OH in global troposphere should remain relatively steady during 2015–2021 (trends: $-0.01\% \text{--} -0.12\% \text{ yr}^{-1}$) (Badia et al., 2021; Q. Li et al., 2022), which is not likely to cause significant declines in GEM concentrations. In addition, a laboratory experiment (at 298 K) showed that gas-phase photooxidation of GEM by atomic Br could shift the GEM isotopic compositions toward lower $\delta^{202}\text{Hg}$ and higher $\Delta^{199}\text{Hg}$ values (G. Sun et al., 2016). In the present study, however, declines in GEM concentrations at MCB and MAL were both accompanied by increasing $\delta^{202}\text{Hg}$ and decreasing $\Delta^{199}\text{Hg}$ values, and therefore cannot be explained by the changes in Br-initiated atmospheric GEM oxidation.

In summary, most factors discussed above, including terrestrial surface emissions, background pool, vegetation activities, and atmospheric oxidation processes, either remained relative constant during the study period or their changes cannot fully explain the synchronous changes in GEM concentrations and isotopic compositions, leaving anthropogenic emissions as a dominant feasible factor causing the continuously decreased GEM concentrations and shifting isotopic compositions in recent years at these two sites. The changes in GEM isotopic compositions with GEM concentrations is systematically consistent at the two investigated sites and are statistically significant for $\Delta^{199}\text{Hg}$ at MCB and $\delta^{202}\text{Hg}$ and $\Delta^{199}\text{Hg}$ at MAL, and such a phenomenon is broadly in agreement with sedimentary and fish records (Lee et al., 2021; Lepak et al., 2019, 2020). For example, Lepak et al. (2019) observed increasing $\delta^{202}\text{Hg}$ and decreasing $\Delta^{199}\text{Hg}$ (e.g., $\sim 0.02\% \text{ yr}^{-1}$) values in fish and sedimentary in Lake Michigan, USA since the early 1990s when regional anthropogenic emissions and atmospheric GEM concentrations started decreasing (Y. X. Zhang et al., 2016). In addition, global sediments showed relatively lower $\Delta^{199}\text{Hg}$ and $\Delta^{200}\text{Hg}$ values in pre-industrial sediments when anthropogenic Hg emissions were low (decreasing by 0.013% decade $^{-1}$ for $\Delta^{199}\text{Hg}$ and 0.0014% decade $^{-1}$ for $\Delta^{200}\text{Hg}$ as compared to present-day value) (Lee et al., 2021; Lepak et al., 2020). Therefore, our observations would probably reflect a regular response of GEM isotopic compositions to reduced anthropogenic emissions. The small changes in GEM isotopic compositions should be attributed to the fact that the difference in the isotopic compositions between anthropogenic emissions and

atmospheric pool (especially for $\Delta^{200}\text{Hg}$) are not sufficiently large, yet such small changes may require appreciable reductions in anthropogenic emissions.

3.3. Contributions of Anthropogenic Emissions to GEM and Its Temporal Changes

GEM in the continental boundary layer could be sourced from anthropogenic emissions, terrestrial surface emissions, and intrusions of air masses from the background free tropospheric pool. $\delta^{202}\text{Hg}$ could be largely shifted by vegetation activities especially at forest sites and is thus not utilized in the mixing model (Fu et al., 2019). Previous high-altitude observational and global modeling studies suggested that photochemical oxidation and reduction of atmospheric Hg have a potential to shift GEM $\Delta^{199}\text{Hg}$ and $\Delta^{200}\text{Hg}$ (Fu, Jiskra, et al., 2021; Song et al., 2022). However, photooxidation and photoreduction rate of atmospheric Hg in the continental boundary layer are typically very low (Horowitz et al., 2017; Shah et al., 2021), and it would not likely change the GEM $\Delta^{199}\text{Hg}$ and $\Delta^{200}\text{Hg}$ significantly during the short-period (less than a few days) atmospheric transport from regional sources to receptors. Here we used a ternary mixing model based on $\Delta^{199}\text{Hg}$ and $\Delta^{200}\text{Hg}$ to estimate the relative contributions of anthropogenic emissions to surface GEM (Equations 3–5), and to probe the changes in regional anthropogenic emissions.

$$\Delta^{199}\text{Hg}_{\text{sample}} = f_{\text{anthro}} \times \Delta^{199}\text{Hg}_{\text{anthro}} + f_{\text{surface}} \times \Delta^{199}\text{Hg}_{\text{surface}} + f_{\text{background}} \times \Delta^{199}\text{Hg}_{\text{background}} \quad (3)$$

$$\Delta^{200}\text{Hg}_{\text{sample}} = f_{\text{anthro}} \times \Delta^{200}\text{Hg}_{\text{anthro}} + f_{\text{surface}} \times \Delta^{200}\text{Hg}_{\text{surface}} + f_{\text{background}} \times \Delta^{200}\text{Hg}_{\text{background}} \quad (4)$$

$$1 = f_{\text{anthro}} + f_{\text{surface}} + f_{\text{background}} \quad (5)$$

where f_{anthro} , f_{surface} , and $f_{\text{background}}$ are the fractions of surface GEM sourced from anthropogenic emissions, terrestrial surface emissions, and background free tropospheric pool, respectively; $\Delta^{199}\text{Hg}_{\text{sample}}$ and $\Delta^{200}\text{Hg}_{\text{sample}}$ are the measured MIF values of GEM samples; $\Delta^{199}\text{Hg}_{\text{anthro}}$ and $\Delta^{200}\text{Hg}_{\text{anthro}}$ are the MIF signatures of anthropogenic emissions estimated from cement, coal, and zinc ores materials ($n = 182$) (Fan et al., 2021; Shen et al., 2019; Yin et al., 2014, 2016); $\Delta^{199}\text{Hg}_{\text{surface}}$ and $\Delta^{200}\text{Hg}_{\text{surface}}$ are the MIF signatures of GEM emitted from terrestrial surfaces (soils and foliage, $n = 61$) (Yuan et al., 2019, 2021; Zhu et al., 2022); and $\Delta^{199}\text{Hg}_{\text{background}}$ and $\Delta^{200}\text{Hg}_{\text{background}}$ are the MIF signatures of GEM from free tropospheric air in the Northern Hemisphere ($n = 20$) (Fu, Jiskra, et al., 2021; Kurz et al., 2020; Nguyen et al., 2021). The median (IQR) $\Delta^{199}\text{Hg}$ and $\Delta^{200}\text{Hg}$ values of the end-members are shown in Figure 5, which encompass most of the observations in the Northern Hemisphere. A Monte Carlo simulation was used to estimate the relative contributions and uncertainties, in which one million groups of $\Delta^{199}\text{Hg}$ and $\Delta^{200}\text{Hg}$ values randomly ranging from IQR of end-members and the analytical uncertainties of the measured $\Delta^{199}\text{Hg}_{\text{sample}}$ and $\Delta^{200}\text{Hg}_{\text{sample}}$ were taken into account.

The contributions of anthropogenic emissions to GEM at MCB and MAL during November 2020 and November 2021 are estimated to be $23 \pm 8\%$ ($0.31 \pm 0.11 \text{ ng m}^{-3}$, mean \pm 1sd) and $31 \pm 15\%$ ($0.46 \pm 0.22 \text{ ng m}^{-3}$, mean \pm 1sd), respectively, which are significantly lower than those at MCB during April 2015 and April 2016 ($29 \pm 9\%$, $0.45 \pm 0.15 \text{ ng m}^{-3}$, mean \pm 1sd) and at MAL during January and December 2017 ($42 \pm 17\%$, $0.70 \pm 0.28 \text{ ng m}^{-3}$, mean \pm 1sd) ($p < 0.05$ at MCB and < 0.01 at MAL, Figure 6; Figure S10 in Supporting Information S1). Terrestrial surface emissions were also responsible for the observed GEM declines at MCB and MAL, likely due to their concurrent changes with reduced anthropogenic emissions and/or less exposures of air mass to the terrestrial surface emissions during 2020/2021, but their declines in GEM concentrations (means: -0.12 – -0.06 ng m^{-3}) were lower than the declines driven by anthropogenic emissions (means: -0.25 – -0.14 ng m^{-3}) (Figure S10 in Supporting Information S1). GEM concentrations sourced from background free tropospheric pool at MCB and MAL showed a slightly increase (means: 0.07 – 0.11 ng m^{-3}), which were likely owing to large exposure of air to non-anthropogenic sources regions during 2020/2021 (Figure S5 in Supporting Information S1). Overall, the above calculations suggest reduction in anthropogenic emissions was the dominant factor causing the GEM declines at MCB and MAL over the past 5–7 years, which can explain 74% and nearly all of the total declined GEM concentrations at MCB from 2015/2016 to 2020/2021 and at MAL from 2017 to 2020/2021.

We acknowledge additional uncertainties in our calculations due to the assumption that the MIF signatures of the ternary end-members sources remained constant over the past years. Besides, other potential sources (e.g., biomass burning and volcanic emissions) were not considered in the calculations because of the lack of sufficient isotopic signatures of their GEM emissions (Duncan et al., 2003; Ebinghaus et al., 2007). We also estimated the relative contributions of anthropogenic emissions to surface GEM in remote China, urban China, Europe, and

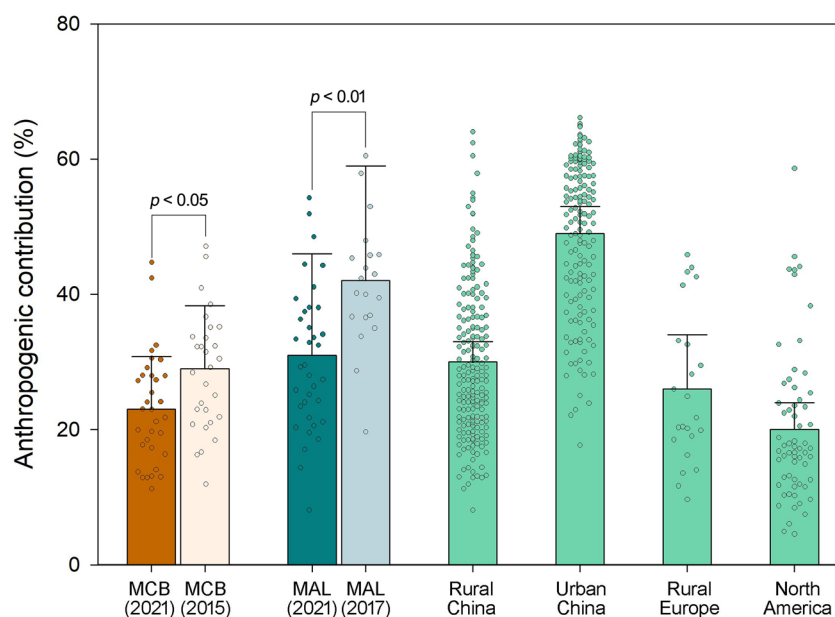


Figure 6. Contributions (mean \pm 1sd) of anthropogenic emissions to gaseous elemental mercury (GEM) at MCB and MAL during the two investigated years, rural and urban sites in China, rural sites in Europe, and North America sites. Data are estimated using a ternary mixing model based on $\Delta^{199}\text{Hg}$ and $\Delta^{200}\text{Hg}$ observed in this and previous studies. Dots are the anthropogenic contributions of each GEM isotope sample.

North America, and obtained mean (\pm 1sd) percentage contributions of $30 \pm 3\%$ ($n = 193$), $49 \pm 4\%$ ($n = 159$), $26 \pm 8\%$ ($n = 23$), and $20 \pm 4\%$ ($n = 62$), respectively (Figure 6). The above values for China (30%–49%) are in a similar range of those generated from modeling studies (on average from 33% to 41%) (Chen et al., 2014; X. Wang et al., 2018), but those for Europe and North America (20%–26%) are higher than previous modeling results (4%–20% from domestic anthropogenic emissions or combustion sources) (Chen et al., 2014; Custódio et al., 2022; Strode et al., 2008), causes for the latter case are attributed to intercontinental transport of anthropogenic emissions (Strode et al., 2008).

Assuming that contributions of anthropogenic emissions to surface GEM respond proportionately to the changes in regional anthropogenic emissions and exposure of air to anthropogenic emissions (Text S3 in Supporting Information S1), we estimated a $5.8 \pm 2.8\%$ yr^{-1} (1sd) decline during 2015–2021 for regional anthropogenic GEM emissions at MCB and a $4.8 \pm 3.0\%$ yr^{-1} (1sd) decline during 2017–2021 at MAL. Despite potential uncertainties in this estimation method due to the simplified assumptions (Text S3 in Supporting Information S1), our results appear to be similar to the decline of total anthropogenic Hg emissions (5.5% yr^{-1}) during 2013–2017 according to the established anthropogenic emission inventory (K. Y. Liu et al., 2019). Emission control measures for air pollutants, especially for SO_2 and $\text{PM}_{2.5}$, were proposed to be major drivers of declining anthropogenic Hg emissions (K. Y. Liu et al., 2019; S. X. Wang et al., 2010; Y. X. Zhang et al., 2016). We found that the declines in anthropogenic Hg emissions reported in the inventory significantly correlated with the declines in surface $\text{PM}_{2.5}$ and SO_2 concentrations in China during 2013–2017 (Figure S12 in Supporting Information S1) (K. Y. Liu et al., 2019; Wei et al., 2021, 2022). Surface $\text{PM}_{2.5}$ and SO_2 concentrations in China continued decreasing after 2017, indicating continued effort of air pollution control measures, which would consequently lead to decreasing anthropogenic Hg emissions in recently years. Using the empirical relationships established during 2013–2017 and taking the decreasing rates of surface $\text{PM}_{2.5}$ and SO_2 concentrations from 2015 to 2020/2021 as input, we would predict an average decline of $5.1 \pm 0.1\%$ yr^{-1} (1sd) in anthropogenic GEM emissions in China from 2015 to 2021, which is overall consistent with the values obtained using the stable Hg isotopes.

4. Conclusions and Environmental Implications

GEM concentrations at two remote sites in China showed continuous decreasing trends over the past 5–7 years, which were mostly likely caused by decreasing regional anthropogenic emissions, as supported by observations

of Hg isotopes. Such a finding is broadly in agreement with modeling studies which showed that atmospheric GEM levels responded quickly to anthropogenic emissions abatements (Amos et al., 2013; K. Y. Liu et al., 2019; Y. X. Zhang et al., 2016). Considering the expected increase in China's anthropogenic Hg emissions before 2015 due to the rapid economic development and its big contribution to the global total anthropogenic Hg emissions (AMAP/UNEP, 2019; K. Y. Liu et al., 2019; Streets et al., 2019a), abatement of anthropogenic Hg emissions in China would have significant impact on global Hg cycling. The observations in this study, together with GEM declines reported in previous studies (Nguyen et al., 2019; Qin et al., 2020; Tang et al., 2018; Wu et al., 2020), indicate the trends in Chinese anthropogenic GEM emissions probably have reversed from early years increasing to recent years declining. Previous studies on Hg emission inventory showed that global anthropogenic Hg emissions increased during 2010–2015, largely (~50%) driven by the increases in East Asia (essentially China) (AMAP/UNEP, 2019; Streets et al., 2019a). Given the large share and rapid decrease of Chinese emissions over the past several years, the declines in China would likely offset or outweighed the increases in other developing regions, subsequently have a potential to result in a reduction of global anthropogenic emissions in recent years.

Results from this study suggest possible changes in isotope compositions of atmospheric Hg pool resulted from changing anthropogenic emissions. The decline in anthropogenic Hg emissions would result in increasing $\delta^{202}\text{Hg}$ and decreasing $\Delta^{199}\text{Hg}$ and $\Delta^{200}\text{Hg}$ values of surface GEM. Since GEM is the dominant form of atmospheric Hg (Horowitz et al., 2017; Shah et al., 2021), the integrated isotope composition of atmospheric Hg pool should respond in a similar direction to that of GEM. A recent study on fish and sediments Hg isotopic compositions in Lake Michigan, USA observed increasing $\delta^{202}\text{Hg}$ and decreasing $\Delta^{199}\text{Hg}$ after 1990 (Lepak et al., 2019), which were likely due to the reduced anthropogenic Hg emissions in USA as a result of the implementation of control measures (Streets et al., 2019b; Y. X. Zhang et al., 2016). In addition, isotope compositions of pre-industrial sediments globally were normally characterized by lower $\Delta^{199}\text{Hg}$ and $\Delta^{200}\text{Hg}$ as compared with present-day sediments (Lee et al., 2021; Lepak et al., 2020). These records require higher $\delta^{202}\text{Hg}$ and lower $\Delta^{199}\text{Hg}$ and $\Delta^{200}\text{Hg}$ signatures for the atmospheric Hg pool under low regional and/or global anthropogenic emissions, which can be essentially explained by our observations.

It is noted that some discrepancies still exist between our observations and sedimentary Hg isotope records. For example, sedimentary records indicate that atmospheric Hg deposition and pool before industrialization likely had relatively lower $\delta^{202}\text{Hg}$ values (Lee et al., 2021; Lepak et al., 2020), in contrast with our observations of increasing GEM $\delta^{202}\text{Hg}$ values under decreasing regional anthropogenic emissions conditions. We speculate that the $\delta^{202}\text{Hg}$ signatures of atmospheric pools may not respond in a uniform direction to the changes in anthropogenic emissions because of the following reasons. (a) Long-term changes in $\delta^{202}\text{Hg}$ of well-processed and well-mixed background atmospheric GEM pool with anthropogenic emissions may differ from those of regional boundary air. Anthropogenic emissions have lower $\delta^{202}\text{Hg}$ than that of background atmospheric pool, and a decrease in regional anthropogenic emissions would therefore have a potential to shift regional $\delta^{202}\text{Hg}_{\text{GEM}}$ values positively as discussed above. Globally, however, large shares of emissions from terrestrial surface, oceans, and geogenic sources in total Hg emissions (>90%) before industrialization could produce lower $\delta^{202}\text{Hg}$ in background atmospheric pool than present-day conditions because of their lower $\delta^{202}\text{Hg}$ signatures than anthropogenic emissions (Selin et al., 2008; R. Y. Sun et al., 2019; Zambardi et al., 2009; Zhu et al., 2022). (b) Pre-industrial anthropogenic emissions had relatively lower $\delta^{202}\text{Hg}$ (R. Y. Sun et al., 2016), which have already been used to interpret the changes of $\delta^{202}\text{Hg}$ in sediments (Lee et al., 2021; Lepak et al., 2020). (c) GEM uptake by foliage and organic soils were not sufficient to drive large positive $\delta^{202}\text{Hg}$ shifts in atmospheric GEM pools before industrialization. Although atmospheric deposition of GEM to foliage and organic soils plays an important role in present-day global Hg cycling and could shift GEM $\delta^{202}\text{Hg}$ values positively (Fu et al., 2019; Jiskra et al., 2018; Selin et al., 2008; Zhou & Obrist, 2021; Zhu et al., 2022), this process is considered to be less important before industrialization due to the much lower ambient levels of GEM (e.g., $<0.5 \text{ ng m}^{-3}$) (Enrico et al., 2017; Fu, Zhu, et al., 2016; Selin et al., 2008), which may explain the relatively lower $\delta^{202}\text{Hg}$ signature in preindustrial atmospheric Hg pool. This hypothesis is supported by the smaller positive or negative shift in $\delta^{202}\text{Hg}_{\text{GEM}}$ during foliar- and soil-atmosphere exchange under low ambient GEM concentrations (Yuan et al., 2019; Zhu et al., 2022). We caution that the links between sedimentary and atmospheric Hg isotope signatures are highly complicated, and many other factors including the changes in deposition pathways, water-atmosphere exchanges, and Hg transformation in atmosphere and water may also affect the trends of Hg isotope composition in both atmospheric pool and sediments. Further knowledge on the mechanisms of these processes and their associated Hg isotope fractionation are needed to better evaluate the changes in anthropogenic emissions and Hg biogeochemical cycling using stable Hg isotope data.

Data Availability Statement

Data discussed in the present study can be found in a public domain repository (<https://doi.org/10.57760/sciencedb.08276>).

Additional information of the ancillary methodology, isotopic compositions of GEM, and temporal changes in environmental factors are presented in the Supporting Information S1 (Text S1–S3, Tables S1–S4, and Figures S1–S12).

Acknowledgments

This work was supported by the Key Research Program of Frontier Science (ZDBS-LY-DQC029) and the Strategic Priority Research Program (XDB4000000), Chinese Academy of Sciences, the National Nature Science Foundation of China (41921004), and the K.C. Wong Education Foundation. We thank the Changbai Mountain and Ailao Mountain Forest Ecosystem research stations, CAS for assistance in collections of atmospheric samples.

References

- Agnan, Y., Le Dantec, T., Moore, C. W., Edwards, G. C., & Obrist, D. (2016). New constraints on terrestrial surface atmosphere fluxes of gaseous elemental mercury using a global database. *Environmental Science & Technology*, *50*(2), 507–524. <https://doi.org/10.1021/acs.est.5b04013>
- AMAP/UNEP. (2013). Geospatially distributed mercury emissions dataset 2010v1 [Dataset]. Arctic Monitoring & Assessment Programme. Retrieved from <https://www.amap.no/mercury-emissions/datasets>
- AMAP/UNEP. (2019). *Technical background report for the global mercury assessment 2018* (pp. viii + 426 pp including E-Annexes). Arctic Monitoring and Assessment Programme, Norway/UN Environment Programme, Chemicals and Health Branch.
- Amos, H. M., Jacob, D. J., Streets, D. G., & Sunderland, E. M. (2013). Legacy impacts of all-time anthropogenic emissions on the global mercury cycle. *Global Biogeochemical Cycles*, *27*(2), 410–421. <https://doi.org/10.1002/gbc.20040>
- Badia, A., Iglesias-Suarez, F., Fernandez, R. P., Cuevas, C. A., Kinnison, D. E., Lamarque, J.-F., et al. (2021). The role of natural halogens in global tropospheric ozone chemistry and budget under different 21st century climate scenarios. *Journal of Geophysical Research: Atmospheres*, *126*(20), e2021JD034859. <https://doi.org/10.1029/2021jd034859>
- Blum, J. D., & Bergquist, B. A. (2007). Reporting of variations in the natural isotopic composition of mercury. *Analytical and Bioanalytical Chemistry*, *388*(2), 353–359. <https://doi.org/10.1007/s00216-007-1236-9>
- Blum, J. D., Sherman, L. S., & Johnson, M. W. (2014). Mercury isotopes in Earth and environmental sciences. *Annual Review of Earth and Planetary Sciences*, *42*, 249–269. <https://doi.org/10.1146/annurev-earth-050212-124107>
- Chen, L., Wang, H. H., Liu, J. F., Tong, Y. D., Ou, L. B., Zhang, W., et al. (2014). Intercontinental transport and deposition patterns of atmospheric mercury from anthropogenic emissions. *Atmospheric Chemistry and Physics*, *14*(18), 10163–10176. <https://doi.org/10.5194/acp-14-10163-2014>
- Cheng, I., Zhang, L., Blanchard, P., Dalziel, J., & Tordon, R. (2013). Concentration-weighted trajectory approach to identifying potential sources of speciated atmospheric mercury at an urban coastal site in Nova Scotia, Canada. *Atmospheric Chemistry and Physics*, *13*(12), 6031–6048. <https://doi.org/10.5194/acp-13-6031-2013>
- Custódio, D., Pfaffhuber, K. A., Spain, T. G., Pankratov, F. F., Strigunova, I., Molepo, K., et al. (2022). Odds and ends of atmospheric mercury in Europe and over the North Atlantic Ocean: Temporal trends of 25 years of measurements. *Atmospheric Chemistry and Physics*, *22*(6), 3827–3840. <https://doi.org/10.5194/acp-22-3827-2022>
- Demers, J. D., Blum, J. D., & Zak, D. R. (2013). Mercury isotopes in a forested ecosystem: Implications for air-surface exchange dynamics and the global mercury cycle. *Global Biogeochemical Cycles*, *27*(1), 222–238. <https://doi.org/10.1002/gbc.20021>
- Demers, J. D., Sherman, L. S., Blum, J. D., Marsik, F. J., & Dvonch, J. T. (2015). Coupling atmospheric mercury isotope ratios and meteorology to identify sources of mercury impacting a coastal urban-industrial region near Pensacola, Florida, USA. *Global Biogeochemical Cycles*, *29*(10), 1689–1705. <https://doi.org/10.1002/2015gb005146>
- Driscoll, C. T., Mason, R. P., Chan, H. M., Jacob, D. J., & Pirrone, N. (2013). Mercury as a global pollutant: Sources, pathways, and effects. *Environmental Science & Technology*, *47*(10), 4967–4983. <https://doi.org/10.1021/es305071v>
- Duncan, B. N., Martin, R. V., Staudt, A. C., Yevich, R., & Logan, J. A. (2003). Interannual and seasonal variability of biomass burning emissions constrained by satellite observations. *Journal of Geophysical Research*, *108*, ACH 1–1–ACH 1–22.
- Ebinghaus, R., Slemr, F., Brenninkmeijer, C. A. M., van Velthoven, P., Zahn, A., Hermann, M., et al. (2007). Emissions of gaseous mercury from biomass burning in South America in 2005 observed during CARIBIC flights. *Geophysical Research Letters*, *34*(8). <https://doi.org/10.1029/2006gl028866>
- Enrico, M., Le Roux, G., Heimbürger, L. E., Van Beek, P., Souhaut, M., Chmeleff, J., & Sonke, J. E. (2017). Holocene atmospheric mercury levels reconstructed from peat bog mercury stable isotopes. *Environmental Science & Technology*, *51*(11), 5899–5906. <https://doi.org/10.1021/acs.est.6b05804>
- Enrico, M., Le Roux, G., Maruszczak, N., Heimbürger, L. E., Claustres, A., Fu, X. W., et al. (2016). Atmospheric mercury transfer to peat bogs dominated by gaseous elemental mercury dry deposition. *Environmental Science & Technology*, *50*(5), 2405–2412. <https://doi.org/10.1021/acs.est.5b06058>
- Fain, X., Obrist, D., Hallar, A. G., Mccubbin, I., & Rahn, T. (2009). High levels of reactive gaseous mercury observed at a high elevation research laboratory in the Rocky Mountains. *Atmospheric Chemistry and Physics*, *9*(20), 8049–8060. <https://doi.org/10.5194/acp-9-8049-2009>
- Fan, H. F., Fu, X. W., Ward, J. F., Yin, R. S., Wen, H. J., & Feng, X. B. (2021). Mercury isotopes track the cause of carbon perturbations in the Ediacaran ocean. *Geology*, *49*(3), 248–252. <https://doi.org/10.1130/g48266.1>
- Fu, X., Jiskra, M., Yang, X., Maruszczak, N., Enrico, M., Chmeleff, J., et al. (2021). Mass-independent fractionation of even and odd mercury isotopes during atmospheric mercury redox reactions. *Environmental Science & Technology*, *55*(14), 10164–10174. <https://doi.org/10.1021/acs.est.1c02568>
- Fu, X., Liu, C., Zhang, H., Xu, Y., Zhang, H., Li, J., et al. (2021). Isotopic compositions of atmospheric total gaseous mercury in 10 Chinese cities and implications for land surface emissions. *Atmospheric Chemistry and Physics*, *21*(9), 6721–6734. <https://doi.org/10.5194/acp-21-6721-2021>
- Fu, X., Yang, X., Tan, Q., Ming, L., Lin, T., Lin, C.-J., et al. (2018). Isotopic composition of gaseous elemental mercury in the marine boundary layer of East China Sea. *Journal of Geophysical Research: Atmospheres*, *123*, 7656–7669. <https://doi.org/10.1029/2018jd028671>
- Fu, X., Zhang, H., Liu, C., Zhang, H., Lin, C.-J., & Feng, X. (2019). Significant seasonal variations in isotopic composition of atmospheric total gaseous mercury at forest sites in China caused by vegetation and mercury sources. *Environmental Science & Technology*, *53*(23), 13748–13756. <https://doi.org/10.1021/acs.est.9b05016>
- Fu, X., Zhu, W., Zhang, H., Sommar, J., Yu, B., Yang, X., et al. (2016). Depletion of atmospheric gaseous elemental mercury by plant uptake at Mt. Changbai, Northeast China. *Atmospheric Chemistry and Physics*, *16*(20), 12861–12873. <https://doi.org/10.5194/acp-16-12861-2016>
- Fu, X., Heimbürger, L. E., & Sonke, J. E. (2014). Collection of atmospheric gaseous mercury for stable isotope analysis using iodine- and chlorine-impregnated activated carbon traps. *Journal of Analytical Atomic Spectrometry*, *29*(5), 841–852. <https://doi.org/10.1039/c3ja50356a>

- Fu, X., Maruszczak, N., Heimburger, L. E., Sauvage, B., Gheusi, F., Prestbo, E. M., & Sonke, J. E. (2016). Atmospheric mercury speciation dynamics at the high-altitude Pic du Midi Observatory, southern France. *Atmospheric Chemistry and Physics*, *16*(9), 5623–5639. <https://doi.org/10.5194/acp-16-5623-2016>
- Gratz, L. E., Keeler, G. J., Blum, J. D., & Sherman, L. S. (2010). Isotopic composition and fractionation of mercury in Great Lakes precipitation and ambient air. *Environmental Science & Technology*, *44*(20), 7764–7770. <https://doi.org/10.1021/es100383w>
- Holmes, C. D., Jacob, D. J., Corbitt, E. S., Mao, J., Yang, X., Talbot, R., & Slemr, F. (2010). Global atmospheric model for mercury including oxidation by bromine atoms. *Atmospheric Chemistry and Physics*, *10*(24), 12037–12057. <https://doi.org/10.5194/acp-10-12037-2010>
- Horowitz, H. M., Jacob, D. J., Zhang, Y. X., Dibble, T. S., Slemr, F., Amos, H. M., et al. (2017). A new mechanism for atmospheric mercury redox chemistry: Implications for the global mercury budget. *Atmospheric Chemistry and Physics*, *17*(10), 6353–6371. <https://doi.org/10.5194/acp-17-6353-2017>
- Jiskra, M., Heimbürger-Boavida, L.-E., Desgranges, M.-M., Petrova, M. V., Dufour, A., Ferreira-Araujo, B., et al. (2021). Mercury stable isotopes constrain atmospheric sources to the ocean. *Nature*, *597*(7878), 678–682. <https://doi.org/10.1038/s41586-021-03859-8>
- Jiskra, M., Sonke, J. E., Agnan, Y., Helmig, D., & Obrist, D. (2019). Insights from mercury stable isotopes on terrestrial-atmosphere exchange of Hg(0) in the Arctic tundra. *Biogeosciences*, *16*(20), 4051–4064. <https://doi.org/10.5194/bg-16-4051-2019>
- Jiskra, M., Sonke, J. E., Obrist, D., Bieser, J., Ebinghaus, R., Myhre, C. L., et al. (2018). A vegetation control on seasonal variations in global atmospheric mercury concentrations. *Nature Geoscience*, *11*(4), 244–250. <https://doi.org/10.1038/s41561-018-0078-8>
- Kurz, A. Y., Blum, J. D., Gratz, L. E., & Jaffe, D. A. (2020). Contrasting controls on the diel isotopic variation of Hg(0) at two high elevation sites in the western United States. *Environmental Science & Technology*, *54*(17), 10502–10513. <https://doi.org/10.1021/acs.est.0c01918>
- Kwon, S. Y., Blum, J. D., Yin, R., Tsui, M. T. K., Yang, Y. H., & Choi, J. W. (2020). Mercury stable isotopes for monitoring the effectiveness of the Minamata Convention on Mercury. *Earth-Science Reviews*, *203*, 103111. <https://doi.org/10.1016/j.earscirev.2020.103111>
- Lee, J. H., Kwon, S. Y., Yin, R., Motta, L. C., Kurz, A. Y., & Nam, S.-I. (2021). Spatiotemporal characterization of mercury isotope baselines and anthropogenic influences in lake sediment cores. *Global Biogeochemical Cycles*, *35*(10), e2020GB006904. <https://doi.org/10.1029/2020gb006904>
- Lei, H., Wuebbles, D. J., Liang, X. Z., Tao, Z., Olsen, S., Artz, R., et al. (2014). Projections of atmospheric mercury levels and their effect on air quality in the United States. *Atmospheric Chemistry and Physics*, *14*(2), 783–795. <https://doi.org/10.5194/acp-14-783-2014>
- Lepak, R. F., Hoffman, J. C., Janssen, S. E., Krabbenhoft, D. P., Ogorek, J. M., DeWild, J. F., et al. (2019). Mercury source changes and food web shifts alter contamination signatures of predatory fish from Lake Michigan. *Proceedings of the National Academy of Sciences of the United States of America*, *116*(47), 23600–23608. <https://doi.org/10.1073/pnas.1907484116>
- Lepak, R. F., Janssen, S. E., Engstrom, D. R., Krabbenhoft, D. P., Tate, M. T., Yin, R., et al. (2020). Resolving atmospheric mercury loading and source trends from isotopic records of remote North American lake sediments. *Environmental Science & Technology*.
- Li, K., Lin, C.-J., Yuan, W., Sun, G., Fu, X., & Feng, X. (2019). An improved method for recovering and preconcentrating mercury in natural water samples for stable isotope analysis. *Journal of Analytical Atomic Spectrometry*, *34*(11), 2303–2313. <https://doi.org/10.1039/c9ja00174c>
- Li, Q., Fernandez, R. P., Hossaini, R., Iglesias-Suarez, F., Cuevas, C. A., Apel, E. C., et al. (2022). Reactive halogens increase the global methane lifetime and radiative forcing in the 21st century. *Nature Communications*, *13*(1), 2768. <https://doi.org/10.1038/s41467-022-30456-8>
- Lindberg, S., Bullock, R., Ebinghaus, R., Engstrom, D., Feng, X. B., Fitzgerald, W., et al. (2007). A synthesis of progress and uncertainties in attributing the sources of mercury in deposition. *Ambio*, *36*(1), 19–32. [https://doi.org/10.1579/0044-7447\(2007\)36\[19:asopau\]2.0.co;2](https://doi.org/10.1579/0044-7447(2007)36[19:asopau]2.0.co;2)
- Liu, C., Fu, X., Xu, Y., Zhang, H., Wu, X., Sommar, J., et al. (2022). Sources and transformation mechanisms of atmospheric particulate bound mercury revealed by mercury stable isotopes. *Environmental Science & Technology*, *56*(8), 5224–5233. <https://doi.org/10.1021/acs.est.1c08065>
- Liu, K. Y., Wu, Q. R., Wang, L., Wang, S. X., Liu, T. H., Ding, D., et al. (2019). Measure-specific effectiveness of air pollution control on China's atmospheric mercury concentration and deposition during 2013–2017. *Environmental Science & Technology*, *53*(15), 8938–8946. <https://doi.org/10.1021/acs.est.9b02428>
- NADP. (2022). National Atmospheric Deposition Program (NADP-3) [Dataset]. NADP Program Office, Wisconsin State Laboratory of Hygiene. Retrieved from <https://nadp.slh.wisc.edu>
- Nguyen, L. S. P., Sheu, G. R., Fu, X. W., Feng, X. B., & Lin, N. H. (2021). Isotopic composition of total gaseous mercury at a high-altitude tropical forest site influenced by air masses from the East Asia continent and the Pacific Ocean. *Atmospheric Environment*, *246*, 118110. <https://doi.org/10.1016/j.atmosenv.2020.118110>
- Nguyen, L. S. P., Sheu, G.-R., Lin, D.-W., & Lin, N.-H. (2019). Temporal changes in atmospheric mercury concentrations at a background mountain site downwind of the East Asia continent in 2006–2016. *Science of the Total Environment*, *686*, 1049–1056. <https://doi.org/10.1016/j.scitotenv.2019.05.425>
- Obrist, D., Agnan, Y., Jiskra, M., Olson, C. L., Colegrove, D. P., Hueber, J., et al. (2017). Tundra uptake of atmospheric elemental mercury drives Arctic mercury pollution. *Nature*, *547*(7662), 201–204. <https://doi.org/10.1038/nature22997>
- Qin, X., Zhang, L., Wang, G., Wang, X., Fu, Q., Xu, J., et al. (2020). Assessing contributions of natural surface and anthropogenic emissions to atmospheric mercury in a fast-developing region of eastern China from 2015 to 2018. *Atmospheric Chemistry and Physics*, *20*(18), 10985–10996. <https://doi.org/10.5194/acp-20-10985-2020>
- Saiz-Lopez, A., Travníkov, O., Sonke, J. E., Thackray, C. P., Jacob, D. J., Carmona-García, J., et al. (2020). Photochemistry of oxidized Hg(I) and Hg(II) species suggests missing mercury oxidation in the troposphere. *Proceedings of the National Academy of Sciences of the United States of America*, *117*(49), 30949–30956. <https://doi.org/10.1073/pnas.1922486117>
- Selin, N. E., Jacob, D. J., Park, R. J., Yantosca, R. M., Strode, S., Jaegle, L., & Jaffe, D. (2007). Chemical cycling and deposition of atmospheric mercury: Global constraints from observations. *Journal of Geophysical Research*, *112*(D2), 1–14. <https://doi.org/10.1029/2006jd007450>
- Selin, N. E., Jacob, D. J., Yantosca, R. M., Strode, S., Jaegle, L., & Sunderland, E. M. (2008). Global 3-D land-ocean-atmosphere model for mercury: Present-day versus preindustrial cycles and anthropogenic enrichment factors for deposition. *Global Biogeochemical Cycles*, *22*(2). <https://doi.org/10.1029/2007gb003040>
- Shah, V., Jacob, D. J., Thackray, C. P., Wang, X., Sunderland, E. M., Dibble, T. S., et al. (2021). Improved mechanistic model of the atmospheric redox chemistry of mercury. *Environmental Science & Technology*, *55*(21), 14445–14456. <https://doi.org/10.1021/acs.est.1c03160>
- Shen, J., Chen, J. B., Algeo, T. J., Yuan, S. L., Feng, Q. L., Yu, J. X., et al. (2019). Evidence for a prolonged Permian-Triassic extinction interval from global marine mercury records. *Nature Communications*, *10*(1), 1563. <https://doi.org/10.1038/s41467-019-09620-0>
- Sheu, G. R., Lin, N. H., Wang, J. L., Lee, C. T., Yang, C. F. O., & Wang, S. H. (2010). Temporal distribution and potential sources of atmospheric mercury measured at a high-elevation background station in Taiwan. *Atmospheric Environment*, *44*(20), 2393–2400. <https://doi.org/10.1016/j.atmosenv.2010.04.009>
- Slemr, F., Brunke, E. G., Ebinghaus, R., & Kuss, J. (2011). Worldwide trend of atmospheric mercury since 1995. *Atmospheric Chemistry and Physics*, *11*(10), 4779–4787. <https://doi.org/10.5194/acp-11-4779-2011>

- Slemr, F., Brunke, E. G., Ebinghaus, R., Temme, C., Munthe, J., Wangberg, I., et al. (2003). Worldwide trend of atmospheric mercury since 1977. *Geophysical Research Letters*, *30*(10). <https://doi.org/10.1029/2003gl016954>
- Smith-Downey, N. V., Sunderland, E. M., & Jacob, D. J. (2010). Anthropogenic impacts on global storage and emissions of mercury from terrestrial soils: Insights from a new global model. *Journal of Geophysical Research*, *115*(G3), G03008. <https://doi.org/10.1029/2009jg001124>
- Song, Z. C., Sun, R. Y., & Zhang, Y. X. (2022). Modeling mercury isotopic fractionation in the atmosphere. *Environmental Pollution*, *307*, 119588. <https://doi.org/10.1016/j.envpol.2022.119588>
- Sprovieri, F., Pirrone, N., Bencardino, M., D'Amore, F., Carbone, F., Cinnirella, S., et al. (2016). Atmospheric mercury concentrations observed at ground-based monitoring sites globally distributed in the framework of the GMOS network. *Atmospheric Chemistry and Physics*, *16*(18), 11915–11935. <https://doi.org/10.5194/acp-16-11915-2016>
- Streets, D. G., Horowitz, H. M., Lu, Z., Levin, L., Thackray, C. P., & Sunderland, E. M. (2019a). Global and regional trends in mercury emissions and concentrations, 2010–2015. *Atmospheric Environment*, *201*, 417–427. <https://doi.org/10.1016/j.atmosenv.2018.12.031>
- Streets, D. G., Horowitz, H. M., Lu, Z., Levin, L., Thackray, C. P., & Sunderland, E. M. (2019b). Five hundred years of anthropogenic mercury: Spatial and temporal release profiles. *Environmental Research Letters*, *14*(8), 084004. <https://doi.org/10.1088/1748-9326/ab281f>
- Strode, S. A., Jaegle, L., Jaffe, D. A., Swartzendruber, P. C., Selin, N. E., Holmes, C., & Yantosca, R. M. (2008). Trans-Pacific transport of mercury. *Journal of Geophysical Research*, *113*(D15), D15305. <https://doi.org/10.1029/2007jd009428>
- Sun, G., Sommar, J., Feng, X., Lin, C.-J., Ge, M., Wang, W., et al. (2016). Mass-dependent and -independent fractionation of mercury isotope during gas-phase oxidation of elemental mercury vapor by atomic Cl and Br. *Environmental Science & Technology*, *50*(17), 9232–9241. <https://doi.org/10.1021/acs.est.6b01668>
- Sun, R. Y., Jiskra, M., Amos, H. M., Zhang, Y. X., Sunderland, E. M., & Sonke, J. E. (2019). Modelling the mercury stable isotope distribution of Earth surface reservoirs: Implications for global Hg cycling. *Geochimica et Cosmochimica Acta*, *246*, 156–173. <https://doi.org/10.1016/j.gca.2018.11.036>
- Sun, R. Y., Streets, D. G., Horowitz, H. M., Amos, H. M., Liu, G. J., Perrot, V., et al. (2016). Historical (1850–2010) mercury stable isotope inventory from anthropogenic sources to the atmosphere. *Elementa: Science of the Anthropocene*, *4*, 1–15. <https://doi.org/10.12952/journal.elementa.000091>
- Sun, W. B., Yang, Y., Chao, L. Y., Dong, W. J., Huang, B. Y., Jones, P., & Li, Q. X. (2022). Description of the China global Merged Surface Temperature version 2.0. *Earth System Science Data*, *14*(4), 1677–1693. <https://doi.org/10.5194/essd-14-1677-2022>
- Swartzendruber, P. C., Jaffe, D. A., Prestbo, E. M., Weiss-Penzias, P., Selin, N. E., Park, R., et al. (2006). Observations of reactive gaseous mercury in the free troposphere at the Mount Bachelor Observatory. *Journal of Geophysical Research*, *111*(D24), D24301. <https://doi.org/10.1029/2006jd007415>
- Tang, Y., Wang, S. X., Wu, Q. R., Liu, K. Y., Wang, L., Li, S., et al. (2018). Recent decrease trend of atmospheric mercury concentrations in East China: The influence of anthropogenic emissions. *Atmospheric Chemistry and Physics*, *18*(11), 8279–8291. <https://doi.org/10.5194/acp-18-8279-2018>
- Tørseth, K., Aas, W., Breivik, K., Fjærraa, A. M., Fiebig, M., Hjellbrekke, A. G., et al. (2012). Introduction to the European Monitoring and Evaluation Programme (EMEP) and observed atmospheric composition change during 1972–2009. *Atmospheric Chemistry and Physics*, *12*, 5447–5481. <https://doi.org/10.5194/acp-12-5447-2012>
- Wang, S. X., Zhang, L., Wu, Y., Ancora, M. P., Zhao, Y., & Hao, J. M. (2010). Synergistic mercury removal by conventional pollutant control strategies for coal-fired power plants in China. *Journal of the Air & Waste Management Association*, *60*(6), 722–730. <https://doi.org/10.3155/1047-3289.60.6.722>
- Wang, X., Lin, C. J., Feng, X. B., Yuan, W., Fu, X. W., Zhang, H., et al. (2018). Assessment of regional mercury deposition and emission outflow in Mainland China. *Journal of Geophysical Research-Atmospheres*, *123*(17), 9868–9890. <https://doi.org/10.1029/2018jd028350>
- Wang, X., Lin, C. J., Yuan, W., Sommar, J., Zhu, W., & Feng, X. B. (2016). Emission-dominated gas exchange of elemental mercury vapor over natural surfaces in China. *Atmospheric Chemistry and Physics*, *16*(17), 11125–11143. <https://doi.org/10.5194/acp-16-11125-2016>
- Wang, Y. Q., Zhang, X. Y., & Draxler, R. R. (2009). TrajStat: GIS-based software that uses various trajectory statistical analysis methods to identify potential sources from long-term air pollution measurement data. *Environmental Modelling & Software*, *24*(8), 938–939. <https://doi.org/10.1016/j.envsoft.2009.01.004>
- Wei, J., Li, Z., Li, K., Dickerson, R. R., Pinker, R. T., Wang, J., et al. (2022). Full-coverage mapping and spatiotemporal variations of ground-level ozone (O₃) pollution from 2013 to 2020 across China. *Remote Sensing of Environment*, *270*, 112775. <https://doi.org/10.1016/j.rse.2021.112775>
- Wei, J., Li, Z., Lyapustin, A., Sun, L., Peng, Y., Xue, W., et al. (2021). Reconstructing 1-km-resolution high-quality PM_{2.5} data records from 2000 to 2018 in China: Spatiotemporal variations and policy implications. *Remote Sensing of Environment*, *252*, 112136. <https://doi.org/10.1016/j.rse.2020.112136>
- Wu, Q., Tang, Y., Wang, S., Li, L., Deng, K., Tang, G., et al. (2020). Developing a statistical model to explain the observed decline of atmospheric mercury. *Atmospheric Environment*, *243*, 117868. <https://doi.org/10.1016/j.atmosenv.2020.117868>
- Wu, Q., Wang, S. X., Li, G. L., Liang, S., Lin, C. J., Wang, Y. F., et al. (2016). Temporal trend and spatial distribution of speciated atmospheric mercury emissions in China during 1978–2014. *Environmental Science & Technology*, *50*(24), 13428–13435. <https://doi.org/10.1021/acs.est.6b04308>
- Yin, R. S., Feng, X. B., & Chen, J. B. (2014). Mercury stable isotopic compositions in coals from major coal producing fields in China and their geochemical and environmental implications. *Environmental Science & Technology*, *48*(10), 5565–5574. <https://doi.org/10.1021/es500322n>
- Yin, R. S., Feng, X. B., Hurley, J. P., Krabbenhoft, D., Lepak, R. F., Hu, R. Z., et al. (2016). Mercury isotopes as proxies to identify sources and environmental impacts of mercury in sphalerites. *Scientific Reports*, *6*(1), 18686. <https://doi.org/10.1038/srep18686>
- Yu, B., Yang, L., Liu, H., Xiao, C., Bu, D., Zhang, Q., et al. (2022). Tracing the transboundary transport of mercury to the Tibetan Plateau using atmospheric mercury isotopes. *Environmental Science & Technology*, *56*(3), 1568–1577. <https://doi.org/10.1021/acs.est.1c05816>
- Yu, B., Yang, L., Liu, H., Yang, R., Fu, J., Wang, P., et al. (2021). Katabatic wind and sea–ice dynamics drive isotopic variations of total gaseous mercury on the Antarctic coast. *Environmental Science & Technology*, *55*(9), 6449–6458. <https://doi.org/10.1021/acs.est.0c07474>
- Yuan, W., Sommar, J., Lin, C.-J., Wang, X., Li, K., Liu, Y., et al. (2019). Stable isotope evidence shows re-emission of elemental mercury vapor occurring after reductive loss from foliage. *Environmental Science & Technology*, *53*(2), 651–660. <https://doi.org/10.1021/acs.est.8b04865>
- Yuan, W., Wang, X., Lin, C. J., Sommar, J. O., Wang, B., Lu, Z. Y., & Feng, X. B. (2021). Quantification of atmospheric mercury deposition to and legacy re-emission from a subtropical forest floor by mercury isotopes. *Environmental Science & Technology*, *55*(18), 12352–12361. <https://doi.org/10.1021/acs.est.1c02744>
- Zambardi, T., Sonke, J. E., Toutain, J. P., Sortino, F., & Shinohara, H. (2009). Mercury emissions and stable isotopic compositions at Vulcano Island (Italy). *Earth and Planetary Science Letters*, *277*(1–2), 236–243. <https://doi.org/10.1016/j.epsl.2008.10.023>

- Zhang, H., Fu, X., Lin, C. J., Shang, L., Zhang, Y., Feng, X., & Lin, C. (2016). Monsoon-facilitated characteristics and transport of atmospheric mercury at a high-altitude background site in southwestern China. *Atmospheric Chemistry and Physics*, *16*(20), 13131–13148. <https://doi.org/10.5194/acp-16-13131-2016>
- Zhang, Y. X., Jacob, D. J., Horowitz, H. M., Chen, L., Amos, H. M., Krabbenhoft, D. P., et al. (2016). Observed decrease in atmospheric mercury explained by global decline in anthropogenic emissions. *Proceedings of the National Academy of Sciences of the United States of America*, *113*(3), 526–531. <https://doi.org/10.1073/pnas.1516312113>
- Zhou, J., & Obrist, D. (2021). Global mercury assimilation by vegetation. *Environmental Science & Technology*, *55*(20), 14245–14257. <https://doi.org/10.1021/acs.est.1c03530>
- Zhu, W., Fu, X., Zhang, H., Liu, C., Skyllberg, U., Sommar, J., et al. (2022). Mercury isotope fractionation during the exchange of Hg(0) between the atmosphere and land surfaces: Implications for Hg(0) exchange processes and controls. *Environmental Science & Technology*, *56*(2), 1445–1457. <https://doi.org/10.1021/acs.est.1c05602>